Nanoscale Advances

ROYAL SOCIETY OF CHEMISTRY

PAPER

View Article Online
View Journal | View Issue

Cite this: *Nanoscale Adv.*, 2025, **7**, 5401

Synergistic design of ZIF-67/Sn-doped NiFe-LDH for enhanced oxygen evolution reaction

Rana Ahmed,[a] Abeer Enaiet Allah,[b] Ahmed A. Farghali,[a] Waleed M. A. El Rouby[a] and Abdalla Abdelwahab *[ac]

The development of efficient and cost-effective oxygen evolution reaction (OER) catalysts is critical for advancing water-splitting technologies. In this study, we report the synthesis of a Sn-doped NiFe layered double hydroxide (LDH) integrated with zeolitic imidazolate framework-67 (ZIF-67)-derived Co species (NiFe-LDH-Sn/ZIF-67) as an efficient catalyst for the OER. The doping of Sn into NiFe-LDH enhances the electronic conductivity and optimizes the active sites for the OER. Concurrently, the introduction of ZIF-67 promotes structural stability and increases the surface area to 727 m^2 g^{-1}, fostering synergistic interactions between the components. The NiFe-LDH-Sn/ZIF-67 catalyst exhibits a significantly lower potential of 1.59 V *vs.* RHE at 10 mA cm^{-2} and a Tafel slope of 79 mV dec^{-1} in alkaline media. The study reveals that Sn doping facilitates the electron transfer process by reducing the equivalent series resistance (ESR) from 325 Ω to 161 Ω, while ZIF-67 improves charge redistribution and catalytic stability by 91.8% after 24 h. This study underscores the potential of combining LDH and metal–organic frameworks to design advanced catalysts for sustainable energy applications.

Received 2nd February 2025
Accepted 10th July 2025

DOI: 10.1039/d5na00113g

rsc.li/nanoscale-advances

Introduction

Despite their historical importance in driving economic and industrial development, fossil fuels present serious social and environmental problems that demand a switch to renewable energy. The burning of fossil fuels such as coal, oil and natural gas is the main source of greenhouse gas emissions, which cause climate change and global warming.[1,2] Therefore, switching to clean energy sources like hydropower, wind, and green hydrogen will reduce these effects and offer a low-emission, sustainable, and renewable substitute to meet the world's energy needs.

Because of its potential as a clean and adaptable energy carrier, hydrogen is becoming a more viable option than fossil fuels.[3,4] Hydrogen produces electricity in fuel cells while releasing only water vapor, removing toxins and greenhouse gases that are produced while burning fossil fuels. It is crucial in some industries, including long-distance transportation, heavy industry such as chemical plants and aviation. However, how hydrogen is produced determines how sustainable it is as a source of energy. Today, the majority of hydrogen is produced from natural gas *via* a method called steam methane reforming, which emits a large amount of CO_2.[5] A switch to green hydrogen produced by electrolysis using renewable energy is necessary to achieve environmental benefits.

Water splitting is a critical process in the production of hydrogen and oxygen. The reaction consists of two half-reactions: the oxidation reaction (oxygen evolution reaction, OER) and the reduction reaction (hydrogen evolution reaction, HER).[6] During the OER, water molecules lose electrons and emit oxygen gas, releasing protons (H^+).[7]

$$2H_2O \rightarrow O_2 + 4H^+ + 4e^- \quad (1)$$

By contrast, in the HER, the protons (H^+) in water gain electrons to generate hydrogen gas.

$$2H^+ + 2e^- \rightarrow H_2 \quad (2)$$

These reactions usually take place in an electrolyzer, where an electric current facilitates the separation of water. Catalysts such as iridium oxide for the OER and platinum for the HER are frequently utilized to improve reaction efficiency.[8,9] Nonetheless, their steep prices encourage continuous investigation into earth-abundant alternatives such as transition metals and layered double hydroxides (LDHs).

Layered double hydroxides (LDHs) are increasingly recognized as promising catalysts for water splitting owing to their impressive performance, adaptable structure, and affordability.[10,11] These materials feature a distinct layered configuration of alternating metal cations and hydroxide layers, offering a unique environment for improving the oxygen

[a]*Materials Science and Nanotechnology Department, Faculty of Postgraduate Studies for Advanced Sciences, Beni-Suef University, Beni-Suef 62511, Egypt. E-mail: aabdelwahab@psas.bsu.edu.eg*

[b]*Chemistry Department, Faculty of Science, Beni-Suef University, Beni-Suef 62511, Egypt*

[c]*Department of Chemistry, College of Sciences, University of Ha'il, Ha'il, 81451, Saudi Arabia. E-mail: a.abdelsalam@uoh.edu.sa*

evolution reaction (OER), a crucial step in the water splitting process.[12,13] LDHs demonstrate high activity and stability owing to their numerous active sites, variable metal compositions, and strong electronic interactions among metals within their layers. By adding transition metals such as nickel, cobalt, and iron, researchers can customize LDHs to enhance catalytic efficiency and lessen the dependence on costly noble metals like iridium.[14,15] NiFe-LDH is a potential catalyst for the OER in an alkaline medium due to the electronic interaction between Fe and OOH, which changes the spin state of Fe, thus decreasing the OER overpotential.[16]

Layered double hydroxides (LDHs) encounter several obstacles in maximizing their effectiveness in the OER. One primary challenge is their relatively low intrinsic conductivity, which can hinder efficient electron transfer and diminish catalytic activity.[17] Moreover, LDHs struggle with stability in the highly oxidative and alkaline environments necessary for the OER because extended use may result in structural degradation or metal ion leaching. Additionally, while enhancing LDH activity using dopants or composites is possible, such modifications often involve compromises due to the cost, performance, and environmental impact. Overcoming these hurdles necessitates innovative strategies in material design, synthesis, and characterization to fully harness the capabilities of LDHs for effective and sustainable OER applications.[18]

The addition of tin (Sn) into layered double hydroxides (LDHs) has proven to be an effective approach for improving their conductivity, which is crucial for enhancing their catalytic efficiency in the OER.[19] Sn, typically introduced as Sn^{4+} ions, alters the electronic structure of LDHs, aiding charge transfer and decreasing resistance at the catalyst surface.[20] This improvement arises from Sn's capability to foster synergistic electronic interactions with transition metals (such as Ni or Co) within the LDH layers, thereby optimizing their redox activity. Furthermore, incorporating Sn can encourage the development of defect sites and increase the availability of active sites, which further enhances catalytic performance. These changes not only boost conductivity but also help maintain the structural integrity of LDHs under challenging electrochemical conditions. In addition, ZIF-67, a cobalt-based zeolitic imidazolate framework, has attracted interest as a precursor for preparing effective catalysts for the oxygen evolution reaction (OER).[21] Its highly porous structure, substantial surface area, and uniform cobalt ion distribution make it an ideal choice for catalytic purposes.[18,22] A. Ahmadi *et al.*[23] studied the synergistic effect of anchoring ZIF-67 onto NiAl-LDH nanosheets to improve the catalytic performance toward the OER. Introducing ZIF-67 into the LDH structure enhances the stability of LDH and increases the active surface area, hence achieving a lower OER overpotential of 190 mV at 20 mA cm^{-2}.

Herein, a composite material Sn-doped NiFe-LDH was prepared and investigated for its electrocatalytic activity toward the OER. Then, this composite was functionalized with ZIF-67 in order to increase the number of available active sites.[24] Therefore, the main objectives of this study are to prepare Sn-doped Ni-Fe LDHs and test their performance towards the OER, along with an evaluation of the role of Sn introduction into NiFe-LDHs and the development of the electrocatalytic activity of Ni-Fe LDHs-Sn *via* the functionalization of the composite with ZIF-67.

2. Materials and methods

2.1. Chemicals

Iron(III) nitrate nonahydrate ($Fe(NO_3)_3 \cdot 9H_2O$, Aladdin), nickel(II) nitrate hexahydrate ($Ni(NO_3)_2 \cdot 6H_2O$, Aladdin), sodium borohydride ($NaBH_4$, Sinopharm Chemical Reagent Co., Ltd), polyvinylpyrrolidone (PVP; $M_w = 40\,000$, Sinopharm Chemical Reagent Co., Ltd), potassium hydroxide (KOH, 99.99%, Aladdin), Vucan XC-72 carbon, dimethylformamide (DMF; Sinopharm Chemical Reagent Co., Ltd) and a Nafion solution (5 wt%, Shanghai Geshu Energy Technology Co., Ltd), $SnCl_2 \cdot 2H_2O$, methanol, $Co(NO_3)_2 \cdot 6H_2O$, and 2-methylimidazole were used. All chemicals were of analytical grade and used as received without any further purification.

2.2. Ni-Fe LDH preparation

Following standard procedures, 0.50 g of PVP was dissolved in 10 mL of a mixture of 0.50 M $Fe(NO_3)_3 \cdot 9H_2O$ and 0.50 M $Ni(NO_3)_2 \cdot 6H_2O$ in equal volumes.[25] After sonication for 10 minutes, the solution was transferred to a beaker containing 50 mL of distilled water. Then, 20 mL of a freshly prepared $NaBH_4$ solution (50 mg mL^{-1}) was added, and the mixture was stirred vigorously at room temperature. The solution's color quickly changed to black, indicating the formation of iron/nickel nanoparticles. As the reaction progressed, the color gradually changed to taupe, suggesting the synthesis of Ni-Fe LDHs. After several hours, the products were collected *via* centrifugation, washed three times with distilled water and once with ethanol, and then dried at 60 °C for 12 hours.

2.3. Ni-Fe LDHs-Sn preparation

0.25 g of Ni-Fe LDHs and 0.25 g of $SnCl_2 \cdot 2H_2O$ were dissolved in 20 mL of methanol. The solution was sonicated for 30 min. 20 mL of a freshly prepared $NaBH_4$ solution (50 mg mL^{-1}) was added to the above solution with vigorous mechanical stirring for 1 hour at room temperature. The products were collected by centrifugation, washed with distilled water and methanol several times, and finally dried at 60 °C overnight.

2.4. Ni-Fe LDHs-Sn/ZIF-67 preparation

0.25 g of Ni-Fe LDH-Sn and $Co(NO_3)_2 \cdot 6H_2O$ (291 mg) were dissolved in 25 mL of methanol to obtain solution A. 2-Methylimidazole (328 mg) was also dissolved in 25 mL of methanol to obtain solution B. Then, solution B was quickly poured into solution A under vigorous agitation for 20 min. The well-mixed solution was aged for 24 h without stirring at room temperature (25 °C). Finally, the purple precipitate (ZIF-67) was washed with absolute methanol four times and then dried in a vacuum oven at 60 °C for 12 h.

2.5. Material characterizations

Scanning electron microscopy (SEM; Hitachi S-4800) and transmission electron microscopy (TEM; Tecnai 20S-TWIN Holland) were used to characterize the morphology and microstructure of the prepared materials. The X-ray diffraction (XRD; Philips X'Pert with Cu Ka radiation) patterns were used for the phase identification of the samples. The surface area and porosity were determined from the nitrogen adsorption–desorption isotherms using Quantachrome TouchWin TM version 1.21. The surface elemental compositions and oxidation states of the samples were analyzed through X-ray photoelectron spectroscopy (XPS; K-ALPHA, Thermo Fisher Scientific, USA).

2.6. Electrochemical measurements

The Autolab PGSTAT302N potentiostat (Metrohm) was used to perform electrochemical measurements utilizing three-electrode cell configurations, and a reference electrode (Ag/AgCl), a counter electrode (graphite rod), and a catalyst-modified glassy carbon (GC) electrode (3 mm diameter) were used. The preparation of the working electrode was as follows: 5 mg of the active material was suspended in 400 μL of isopropanol and 10 μL of a Nafion solution, which was added as a binding material. The suspension was ultrasonicated for 30 minutes; then, 10 μL of the suspension was spread onto the cleaned (GC) electrode tip. Finally, the electrode was dried at 40 °C for 30 minutes. Before the OER electrochemical tests, the electrolyte was purged with an oxygen gas flow for 30 minutes. All measurements were recorded using NOVA software (version 1.11), in a 1 M KOH solution. The performed electrochemical measurements were linear sweep voltammetry (LSV), cyclic voltammetry (CV), chronoamperometry (CA), and electrochemical impedance spectroscopy (EIS). LSV was performed at a scan rate of 5 mV s^{-1} in a potential range from 0 to 1 V. CV was recorded in the potential range between 0.6 V and 1.82 V *vs.* RHE at a scan rate of 20 mV s^{-1}. The CA stability test was performed at 1.32 V *vs.* RHE for 24 h. EIS was conducted with a 10-mV amplitude in the frequency range from 100 kHz to 0.05 Hz. Finally, the Ag/AgCl electrode was calibrated to the reversible hydrogen electrode (RHE) using the following equation:

$$E_{RHE} = E_{Ag/AgCl} + 0.1976 + 0.059 \times pH$$

where E_{RHE} refers to the potential *vs.* RHE, $E_{Ag/AgCl}$ is the measured potential *vs.* Ag/AgCl, and pH is the pH of the alkaline medium (1 M KOH).

3. Results and discussion

3.1 Preparation scheme

Fig. 1 shows the preparation scheme for NiFe-LDH-Sn/ZIF-67, where PVP and $NaBH_4$ were added to 10 mL of $Fe(NO_3)_3 \cdot 9H_2O$ and $Ni(NO_3)_3 \cdot 9H_2O$. The solution was vigorously stirred to obtain NiFe LDH. Then, $SnCl_2 \cdot 2H_2O$ was added to obtain Sn-doped NiFe LDH (NiFe LDH-Sn). The presence of Sn nanoparticles between the LDH layers promotes the formation of active sites for oxygen adsorption and reduces the agglomeration of LDH layers. Finally, $Co(NO_3)_2 \cdot 6H_2O$ and 2-methylimidazole were added to NiFe LDH-Sn to functionalize with ZIF-67. This structure has several advantages, including a high surface area, a high content of active sites, and high stability, suggesting its potential use as an electrocatalyst for the OER.

3.2 Morphological characterization

Fig. 2a shows the FESEM image of NiFe-LDH, in which the flower-like morphology is observed. This structure results from the self-assembly of nanosheets extending outward.[26] These flower-like clusters offer an extensive surface area and improve access to active areas, which is advantageous for applications such as catalysis and electrochemical processes. The interstitial spaces among the stacked or assembled nanosheets form a mesoporous structure. These pores are crucial for enhancing ion diffusion and material accessibility in energy storage or catalytic applications. Fig. 2b shows the SEM image of NiFe-LDH-Sn, in which smaller flower-like clusters can be observed because Sn doping improves hierarchical structures by preventing aggregation and facilitating the formation of smaller, well-defined sheet clusters.[19,20] The NiFe-LDH-Sn/ZIF-67 images are presented in Fig. 2c and d at different magnifications. As can be seen, the growth of ZIF-67 on the NiFe-LDH-Sn surface occurs in the form of dodecahedral crystals that are heterogeneous in size.[27] ZIF-67 crystals are typically dispersed individually, but they may agglomerate based on the drying or washing procedures employed during synthesis. These aggregates maintain interparticle spaces, which may enhance porosity. In addition, the polyhedral structure guarantees the consistent exposure of active sites and facilitates uniform catalytic activity.[18,22]

EDX analysis (Fig. 2e) shows the presence of the target elements in NiFe-LDH-Sn/ZIF-67, which are C, O, Sn, Fe, Co, and Ni. Moreover, the elemental mapping analysis (Fig. 2f–k) reveals the homogenous distribution of the targeted elements. Fig. 2l shows the HRTEM image of NiFe-LDH-Sn/ZIF-67, in which thin, layered NiFe-LDH nanosheets are closely integrated with crystalline ZIF-67 nanoparticles. The ZIF-67 particles are uniformly anchored onto the nanosheets, exhibiting discernible lattice fringes and robust interfacial contacts.

3.3 Surface area and XRD analysis

Fig. 3a and b shows the N_2 adsorption–desorption isotherms of the prepared samples and the corresponding Barrett–Joyner–Halenda (BJH) pore size distributions, respectively. In Fig. 3a, the obtained isotherms are of type II isotherms.[28] At low relative pressure, the isotherm exhibits an increase in the quantity of gas adsorbed due to the monolayer adsorption of nitrogen molecules on the internal and external surfaces of the material. At moderate relative pressure, the adsorption increases to form multiple layers on the pore walls. By contrast, at high relative pressure, a hysteresis loop is observed due to capillary condensation. The hysteresis loop is of the H3 type, which exhibits the non-rigid aggregates of plate-like particles or macroporous networks that are not fully filled with the

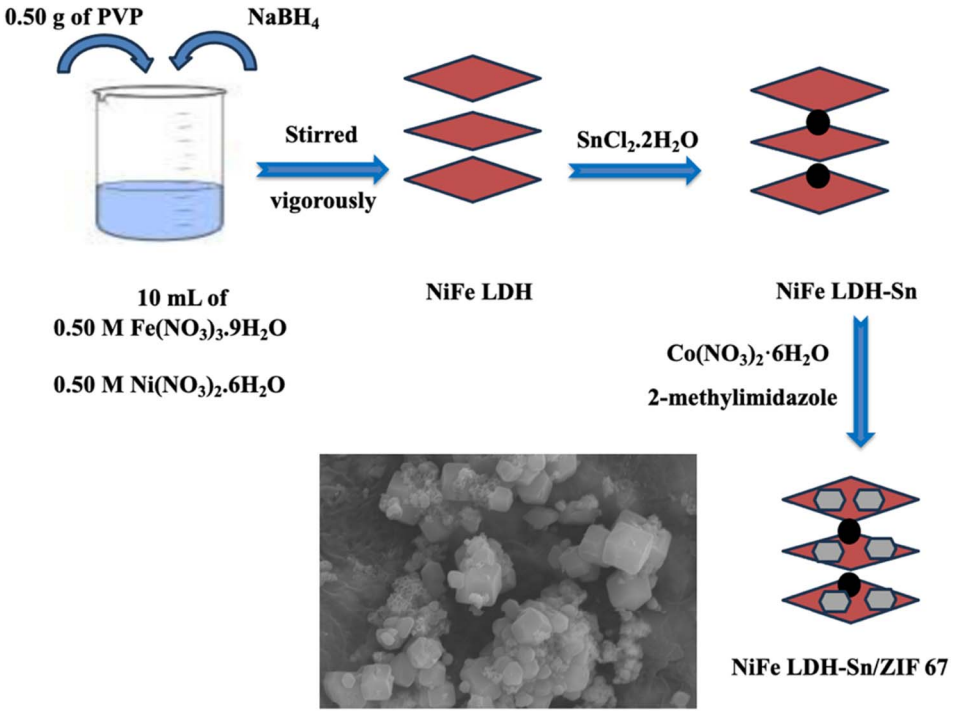

Fig. 1 Preparation scheme for NiFe-LDH-Sn/ZIF-67.

condensate. The quantity of gas adsorbed is higher in NiFe-LDH-Sn/ZIF 67, indicating the higher surface area of this sample, which reaches 727 $m^2 g^{-1}$ (Table 1). Moreover, the pore size distribution was obtained by applying the BJH model to the desorption part of the N_2 isotherm (Fig. 3b). The BJH pore size distribution reveals that all materials are in the mesoporous range, and most of the pores are in the range from 2.5 nm to 10 nm, with a higher concentration of mesopores in NiFe-LDH-Sn/ZIF-67. The presence of mesopores facilitates the diffusion of electrolytic ions inside the material's structure and develops

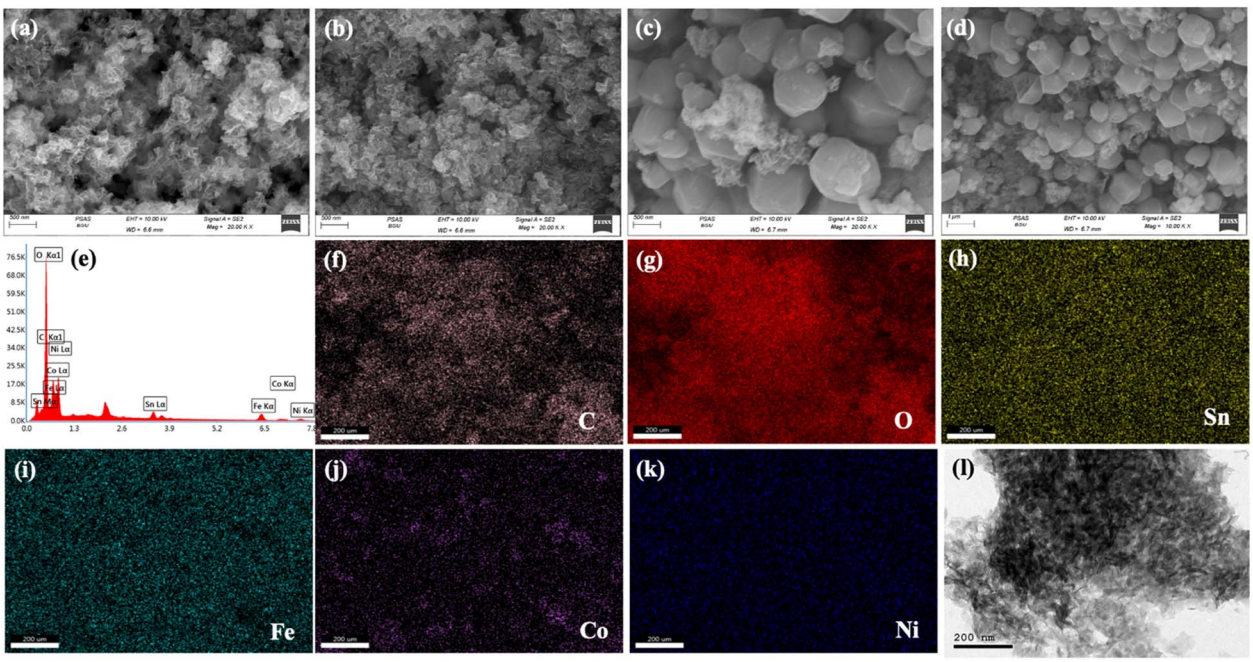

Fig. 2 FESEM images of (a) NiFe-LDH, (b) NiFe-LDH-Sn, and (c and d) NiFe-LDH-Sn/ZIF-67. (e) EDX analysis, (f–k) elemental mapping, and (l) HRTEM image of NiFe-LDH-Sn/ZIF-67.

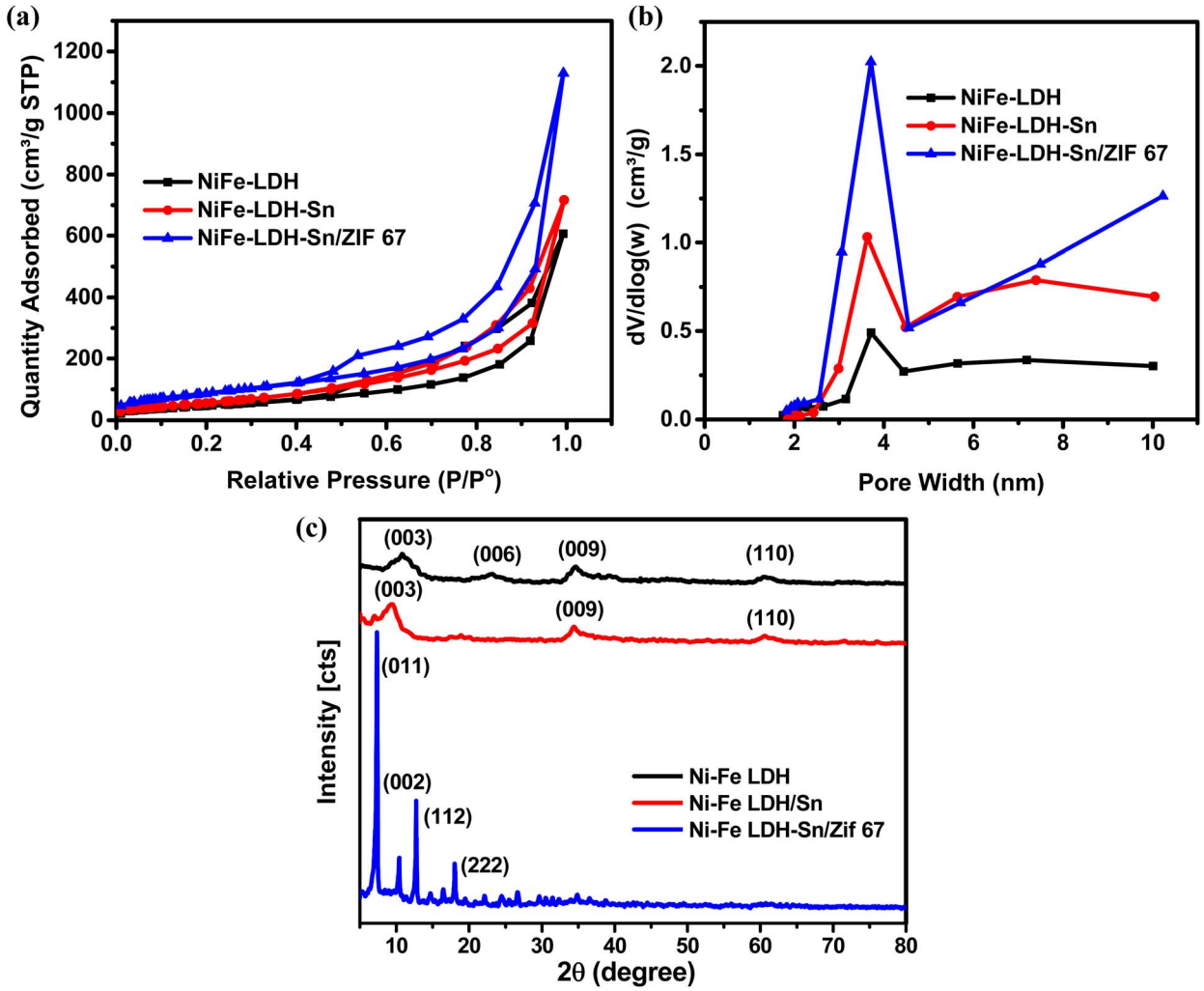

Fig. 3 (a) N_2 adsorption–desorption isotherms of all prepared samples, (b) BJH pore size distributions, and (c) XRD patterns of the synthesized materials.

Table 1 Data obtained from the surface area analysis[a]

Electrocatalysts	L_o (nm)	S_{BET} ($m^2\ g^{-1}$)
Ni-Fe LDH	5.3	173
Ni-Fe LDH/Sn	5.4	322
Ni-Fe LDH-Sn/ZIF 67	5.7	727

[a] L_o: pore diameter; S_{BET}: BET specific surface area.

catalytically active sites, hence diminishing mass transfer constraints.

Fig. 3c shows the XRD patterns of the prepared samples. The diffraction pattern of NiFe LDH exhibits diffraction peaks at 2θ values of 11.82°, 23.33°, 35.01°, and 63.24°, which correspond to the (003), (006), (009), and (110) planes, respectively. These diffraction peaks are the characteristic peaks of nickel–iron layered double hydroxides (JCPDS no. 40-0215).[29] Moreover, the addition of Sn to NiFe LDH causes the main peak (003) to shift to lower 2θ values, indicating the incorporation of Sn between NiFe LDH layers. Furthermore, the presence of the characteristic diffraction peaks of ZIF-67 confirms the successful integration of ZIF-67 into NiFe LDH-Sn. The main peaks of ZIF-67 are positioned at 2θ values of 7.2°, 10.4°, 12.7°, 14.7°, 16.4°, and 18°, which are assigned to the (011), (002), (112), (022), (013), and (222) planes, respectively.[30]

X-ray photoelectron spectroscopy (XPS) is an effective technique for examining the surface elemental composition and chemical states within a material. Fig. 4 presents the XPS spectra of NiFe-LDH-Sn/ZIF-67. The Ni 2p spectrum (Fig. 4a) shows the two spin–orbit doublets of Ni $2p_{3/2}$ and Ni $2p_{1/2}$, where the Ni^{2+} peaks are located at 855.7/873.4 eV with two satellite peaks at 861.7/880.3 eV, respectively.[31] In addition, the Ni^{3+} peaks are located at 858.44/875.05 eV, with two satellite peaks at 864.87/883.18 eV. The presence of Ni^{3+}, in addition to Ni^{2+} ions, plays a crucial role in developing the OER catalytic process.[31] The Fe 2p spectrum confirms the existence of Fe^{2+} and Fe^{3+} (Fig. 4b). There are two peaks for Fe^{2+} at 712.6/724.5 eV for Fe $2p_{3/2}$ and Fe $2p_{1/2}$, respectively.[31,32] Similarly, there are two peaks for Fe^{3+} at 714.5/727.4 eV, respectively. The satellite peaks for Fe 2p are located at 718.0, 720.9, and 732.44 eV. For Sn

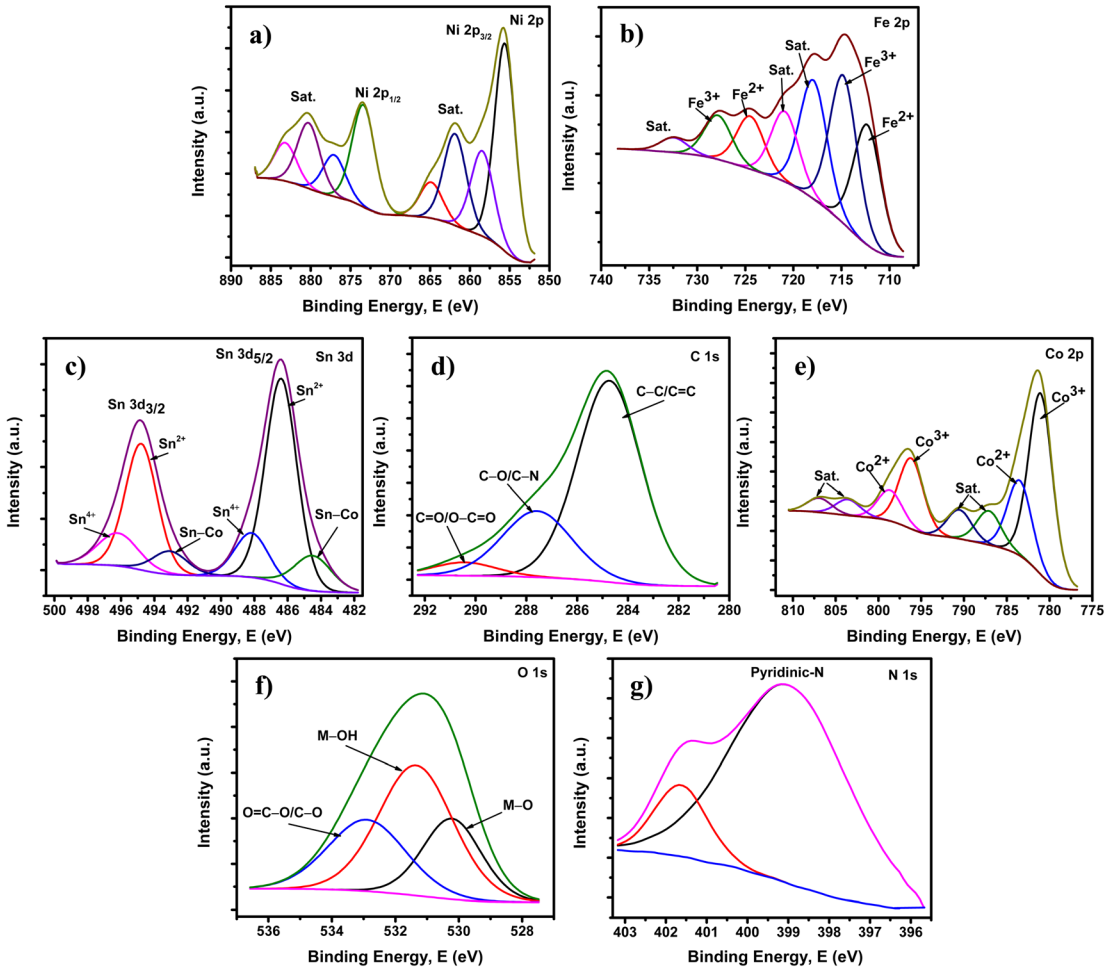

Fig. 4 (a) Ni 2p, (b) Fe 2p, (c) Sn 3d, (d) C 1s, (e) Co 2p, (f) O 1s, and (g) N 1s XPS spectra of NiFe-LDH-Sn/ZIF-67.

species (Fig. 4c), there are two peaks located at 484.5 and 493.08 eV, which may be assigned to the Sn–Co bond, indicating the successful integration of Sn in ZIF-67.[33,34] Furthermore, the deconvoluted peaks at 486.39/494.8 eV and 488.1/496.2 eV are ascribed to Sn^{2+} and Sn^{4+} with Sn $3d_{5/2}$ and Sn $3d_{3/2}$, respectively. It is well noted that the presence of Sn^{4+} ions can enhance conductivity by decreasing the resistance on the LDH surface.[19,20] Fig. 4d shows the C 1s spectrum with three deconvoluted peaks centered at 284.7, 287.6, and 290.7 eV, which are assigned to C=C/C–C, C–O/C–N, and C=O/O–C=O, respectively, suggesting the presence of oxidized carbon species likely introduced during synthesis or from residual organic ligands.[32]

Fig. 4e reveals the XPS spectrum of Co 2p, where the two species of Co^{3+} and Co^{2+} are present. For Co^{3+}, there are two peaks centered at 781.03 and 796.4 eV, along with two satellite peaks at 787.2 and 803.7 eV. In addition, the Co^{2+} peaks are located at 783.8 and 798.8 eV, and their satellite peaks are located at 790.54 and 807.1 eV.[31] The three peaks in the O 1s spectrum (Fig. 4f) are located at 530.22, 531.35, and 533.0, corresponding to the metal–oxygen bond (M–O), hydroxyl–oxygen bond (M–OH), and C–O or O=C–O bond, respectively.[33] The XPS spectrum of N 1s (Fig. 4g) reveals a prominent peak centered at approximately 399.3 eV, which is attributed to pyridinic-type nitrogen from the imidazolate linkers in the ZIF-67 framework, confirming the structural integrity of the MOF component within the composite. In addition, a secondary peak at ~401.7 eV is observed, which is not characteristic of pyrrolic nitrogen but is more likely assigned to protonated nitrogen species ($-NH^{+}$) or nitrogen atoms involved in strong interactions with metal cations. The presence of this higher-binding-energy feature suggests a degree of electronic interaction between ZIF-67 and the LDH matrix, possibly due to the interfacial charge redistribution or partial coordination of nitrogen with metal centers. Table 2 summarizes the binding energy, elemental atomic %, and full width at half-maximum (FWHM) of the targeted elements. From the abovementioned results, the XPS spectral analysis confirms the successful preparation of NiFe-LDH-Sn/ZIF-67.

3.4 OER evaluation

In order to evaluate the activity of the prepared materials towards the OER, the electrocatalytic performance of NiFe-LDH, NiFe-LDH-Sn, and NiFe-LDH-Sn/ZIF-67 was studied in 1 M KOH using linear sweep voltammetry (LSV) measurements. Fig. 5a

Table 2 Calculated binding energies, FWHM, and atomic % of the elements from the integrated peak area

XPS spectra	Binding energy, eV	FWHM	Atomic %
C 1s	284.67	3.67	15.20
O 1s	531.08	3.89	41.40
N 1s	399.08	3.29	0.56
	401.28	1.28	
Ni 2p	855.78	4.69	10.17
	861.78	4.87	
	873.48	4.44	
	880.38	7.70	
Fe 2p	714.58	5.28	11.98
	717.68	6.20	
	724.38	3.40	
	727.38	4.20	
Co 2p	781.38	4.72	18.80
	790.18	3.70	
	796.48	5.48	
Sn 3d	486.38	2.67	1.89
	494.88	2.75	

shows the LSV polarization curves obtained at a scan rate of 5 mV s^{-1}. NiFe-LDH-Sn/ZIF-67 shows an obviously higher activity for the OER than other samples. As shown, NiFe-LDH-Sn/ZIF-67 can achieve a current density of 10 mA cm^{-2} by consuming a lower overpotential of 1.59 V. By contrast, for NiFe-LDH and NiFe-LDH-Sn, the overpotentials reach 1.99 V and 1.68 V, respectively. This indicates that the doping of NiFe-LDH with Sn and ZIF-67 can enhance the electrocatalytic activity toward the OER by improving the LDH conductivity and promoting its surface area.[29]

Moreover, the Tafel slope is an essential kinetic measure for elucidating alterations in the OER mechanism. A reduced Tafel slope indicates accelerated OER kinetics.[31] Fig. 5b shows the Tafel slopes of NiFe-LDH, NiFe-LDH-Sn, and NiFe-LDH-Sn/ZIF-67, where the lowest Tafel slope is observed for NiFe-LDH-Sn/ZIF-67, with a value of 79 mV dec^{-1}. By contrast, for NiFe-LDH and NiFe-LDH-Sn, the Tafel slopes are found to be 290 mV dec^{-1} and 140 mV dec^{-1}, respectively, indicating that the NiFe-LDH-Sn/ZIF-67 electrocatalyst has fast OER kinetics.

Fig. 5c shows the cyclic voltammetry (CV) profiles of the NiFe-LDH-Sn/ZIF-67 composite recorded under N_2- and O_2-saturated alkaline conditions to assess its electrocatalytic activity toward the OER. Under N_2-saturated conditions, the CV profile of the NiFe-LDH-Sn/ZIF-67 composite exhibits a single well-defined cathodic peak at approximately 1.1 V *vs.* RHE, which is attributed to the $Co^{3+} \rightarrow Co^{2+}$ reduction process. This peak reflects the intrinsic redox activity of the cobalt centers in the absence of oxygen. Upon saturation with O_2, a significant increase in the anodic current is observed at potentials above

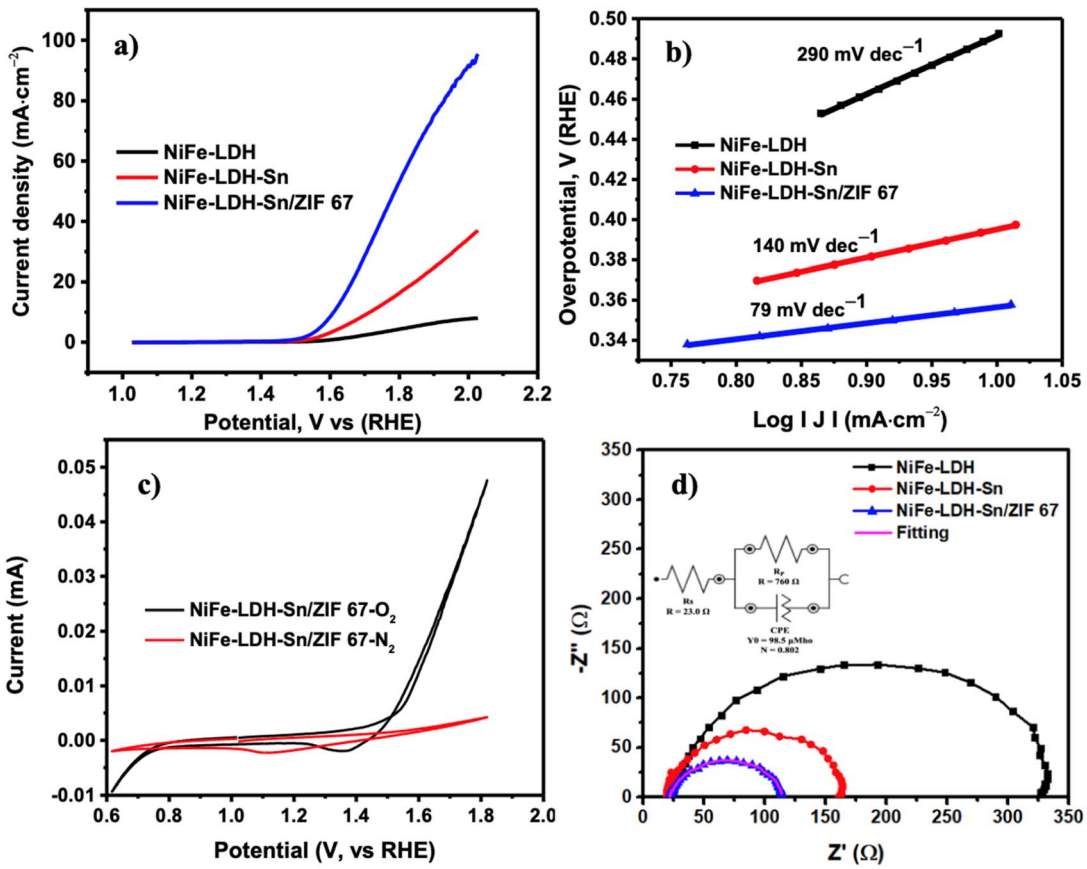

Fig. 5 (a) LSV curves in 1 M KOH at a scan rate of 5 mV s^{-1}, (b) Tafel plots, (c) CV curves for NiFe-LDH-Sn/ZIF 67 in N_2- and O_2-saturated 1 M KOH, and (d) Nyquist plots at 0.5 V.

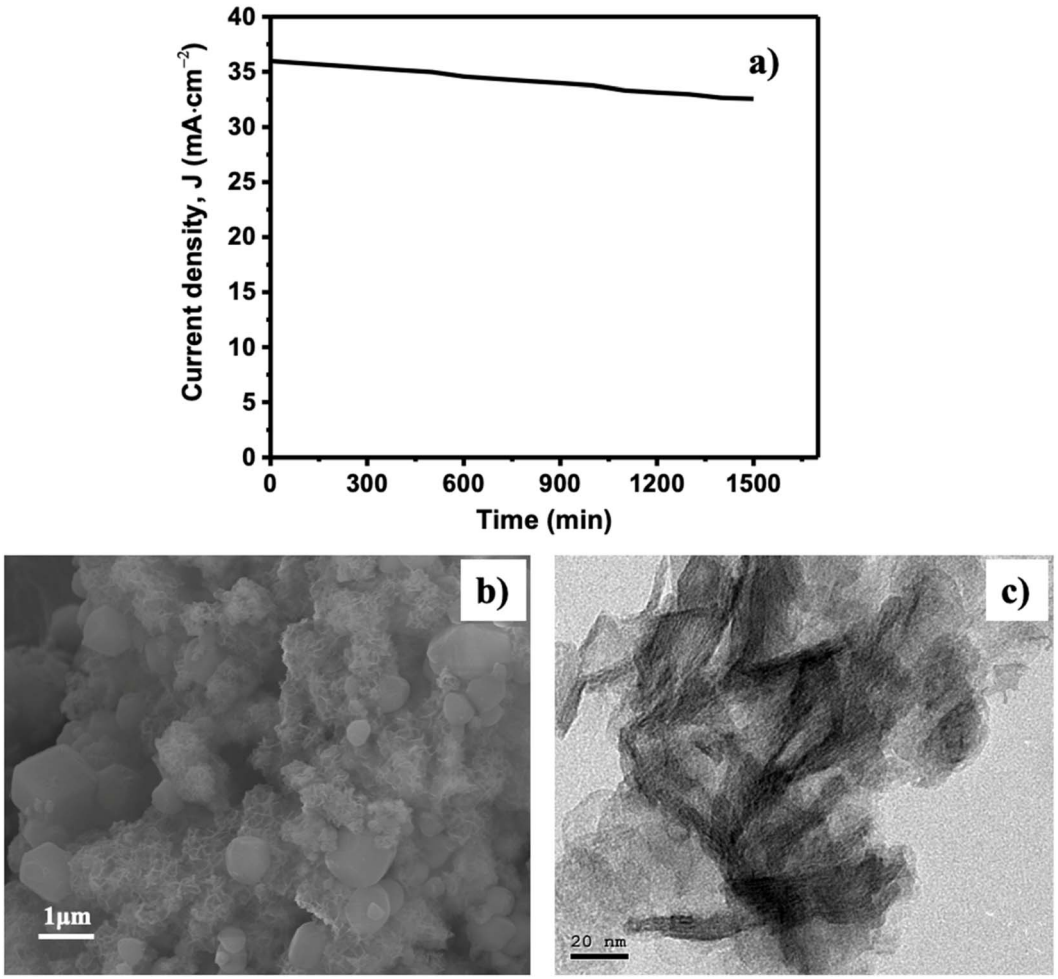

Fig. 6 (a) Stability test for 24 h, (b) post-FESEM characterization, and (c) post-HRTEM characterization images of NiFe-LDH-Sn/ZIF-67.

~1.5 V *vs.* RHE, which is indicative of pronounced OER activity. Interestingly, under O_2-saturated conditions, the reduction peak observed in the N_2-saturated electrolyte shifts positively to ~1.4 V, suggesting a change in the local redox environment and electronic structure of the active sites in the presence of molecular oxygen. The positive shift may be indicative of the surface oxidation or stabilization of higher-valent cobalt species (Co^{4+}) due to oxygen adsorption or intermediate formation during the OER. This shift highlights the interaction between the catalyst and oxygen species and may also suggest the presence of enhanced oxidizing conditions on the catalyst surface during the OER, contributing to the overall improved electrocatalytic performance.

Electrochemical impedance spectroscopy (EIS) is an important technique for determining the conductivity and resistance of an electrode. Fig. 5d presents the Nyquist plots of the prepared materials, where a semicircle is obtained at a high frequency range at 0.5 V. The width and height of the semicircle in a Nyquist plot yield essential information regarding the conductivity and electrochemical characteristics of a substance.[35] In impedance spectroscopy, the semicircle generally signifies the bulk response of the material, encompassing its resistance and capacitance. The width of the semicircle correlates directly with the bulk resistance (R_b) of the material; a narrower semicircle signifies reduced resistance and thus enhanced conductivity.[36] By contrast, the height of the semicircle represents dielectric relaxation processes and capacitance, indicating the material's capacity to store and transport charge. An increased height frequently indicates substantial polarization effects or interfacial resistance, potentially diminishing effective conductivity. As shown in Fig. 5d, the reduced width and height of the semicircle are observed for NiFe-LDH-Sn/ZIF-67, indicating higher conductivity and lower resistance. The inset in Fig. 5d shows the equivalent circuit model used to fit the EIS data, where the calculated equivalent series resistances (ESRs) for NiFe-LDH, NiFe-LDH-Sn, and NiFe-LDH-Sn/ZIF-67 are 325 Ω, 161 Ω, and 115 Ω, respectively. The use of the CPE instead of an ideal capacitor accounts for the non-ideal electrochemical double layer behavior, which is commonly observed in porous or heterogeneous electrodes. The calculated solution resistance (R_s) equals 23 Ω.

Furthermore, the stability test in OER research is an essential assessment criterion for evaluating the long-term performance and durability of electrocatalysts under operational

settings. The stability test is performed *via* chronoamperometry, which tracks the catalyst's performance over 24 h (Fig. 6a). Negligible variations in the catalytic current density are observed, with a retention reaching 91.8%. In addition, the stability is affected by phenomena like catalyst dissolution, surface oxidation, and detachment from the electrode substrate, which may impair performance. Therefore, post-FESEM and HRTEM characterization analyses were performed for NiFe-LDH-Sn/ZIF-67 (Fig. 5b and c). The post-FESEM and HRTEM characterization results reveal the stability of the morphology of NiFe-LDH-Sn/ZIF-67 in the used electrolyte after the long-term stability test, suggesting the potential use of this electrode as an electrocatalyst for the OER.

Conclusions

In this study, we successfully prepared an effective OER catalyst by doping Sn into NiFe-LDH and integrating it with ZIF-67. Sn doping markedly improved electronic conductivity and optimized active sites for the OER, whereas ZIF-67 enhanced the structural stability and surface area, facilitating synergistic catalytic performance. The NiFe-LDH-Sn/ZIF-67 catalyst exhibited exceptional OER activity, characterized by a minimal overpotential, an advantageous Tafel slope, and remarkable stability in alkaline environments. These findings underscore the potential of integrating doped layered double hydroxides with metal–organic framework-derived materials to develop enhanced electrocatalysts for sustainable energy applications. This method offers a viable avenue for creating economical, high-efficiency catalysts for water splitting and other applications.

Data availability

The data supporting this article have been included as part of the main manuscript.

Conflicts of interest

There are no conflicts to declare.

References

1 M. Mhadhbi, The interconnected carbon, fossil fuels, and clean energy markets: Exploring Europe and China's perspectives on climate change, *Finance Res. Lett.*, 2024, **62**, 105185.
2 A. Heras and J. Gupta, Fossil fuels, stranded assets, and the energy transition in the Global South: A systematic literature review, *WIREs Clim. Change*, 2024, **15**(1), e866.
3 H. Zhou, *et al.*, Understanding innovation of new energy industry: Observing development trend and evolution of hydrogen fuel cell based on patent mining, *Int. J. Hydrogen Energy*, 2024, **52**, 548–560.
4 T. L. Oladosu, *et al.*, Energy management strategies, control systems, and artificial intelligence-based algorithms development for hydrogen fuel cell-powered vehicles: A review, *Int. J. Hydrogen Energy*, 2024, **61**, 1380–1404.
5 M. Liu, *et al.*, Enhanced hydrogen production of mid-temperature chemical looping steam methane reforming using lithium-based sorbent particles, *Chem. Eng. J.*, 2024, **498**, 155522.
6 B. You and Y. Sun, Innovative Strategies for Electrocatalytic Water Splitting, *Acc. Chem. Res.*, 2018, **51**(7), 1571–1580.
7 H. Sun, *et al.*, Advanced electrocatalysts with unusual active sites for electrochemical water splitting, *InfoMat*, 2024, **6**(1), e12494.
8 M. Kost, *et al.*, Chemical Epitaxy of Iridium Oxide on Tin Oxide Enhances Stability of Supported OER Catalyst, *Small*, 2024, **20**(42), 2404118.
9 N. Wang, *et al.*, Titanium dioxide supported low-loading platinum as efficient and durable electrocatalyst for acidic hydrogen evolution reaction, *Mol. Catal.*, 2024, **564**, 114327.
10 S. Dresp, *et al.*, Efficient direct seawater electrolysers using selective alkaline NiFe-LDH as OER catalyst in asymmetric electrolyte feeds, *Energy Environ. Sci.*, 2020, **13**(6), 1725–1729.
11 S. Liu, *et al.*, Boosting oxygen evolution activity of NiFe-LDH using oxygen vacancies and morphological engineering, *J. Mater. Chem. A*, 2021, **9**(41), 23697–23702.
12 D. Liu, *et al.*, Improved OER catalytic performance of NiFe-LDH with hydrothermal carbonization microspheres, *J. Alloys Compd.*, 2023, **941**, 168994.
13 Z.-Y. Liu, *et al.*, Conjugated polycarboxylate ligand-coordinated NiFe LDH for enhanced oxygen evolution, *J. Mater. Chem. A*, 2024, **12**(40), 27497–27505.
14 Y. Wang, *et al.*, Atomically targeting NiFe LDH to create multivacancies for OER catalysis with a small organic anchor, *Nano Energy*, 2021, **81**, 105606.
15 X.-J. Zhai, *et al.*, Advances in the design of highly stable NiFe-LDH electrocatalysts for oxygen evolution in seawater, *Chem. Eng. J.*, 2024, **496**, 153187.
16 Q. Lin, *et al.*, Oxygen evolution reaction on NiFe-LDH/(Ni,Fe)OOH: theoretical insights into the effects of electronic structure and spin-state evolution, *Phys. Chem. Chem. Phys.*, 2025, **27**(9), 4926–4933.
17 D. Tyndall, *et al.*, Demonstrating the source of inherent instability in NiFe LDH-based OER electrocatalysts, *J. Mater. Chem. A*, 2023, **11**(8), 4067–4077.
18 K. Wang, *et al.*, Rational Design of a Novel S-Scheme Heterojunction based on ZIF-67-Supported Ni-Fe Layered Double Hydroxide for Efficient Photocatalytic Hydrogen Generation, *Energy Fuels*, 2022, **36**(4), 2058–2067.
19 Y. Sun, *et al.*, Two-Dimensional SnS Mediates NiFe-LDH-Layered Electrocatalyst toward Boosting OER Activity for Water Splitting, *ACS Appl. Mater. Interfaces*, 2024, **16**(18), 23054–23060.
20 S. Velu, *et al.*, Effect of Sn Incorporation on the Thermal Transformation and Reducibility of M(II)Al-Layered Double Hydroxides [M(II) = Ni or Co], *Chem. Mater.*, 2000, **12**(3), 719–730.
21 X. Guo, *et al.*, An in situ formed ZIF-67 derived NiFeCo-P nano-array for accelerating the electrocatalytic oxygen evolution reaction, *Energy Adv.*, 2024, **3**(3), 654–663.

22 Z. Lin, *et al.*, ZIF-67-derived FeCoNi-LDH with a 3D nanoflower hierarchical structure for highly efficient oxidation of 5-Hydroxymethylfurfural and coupling seawater splitting hydrogen production, *Chem. Eng. J.*, 2024, **481**, 148429.
23 A. Ahmadi, *et al.*, Synergistic ZIF-67(Co) anchoring NiAl-LDH nanosheets: Morphology transformation for efficient electrocatalytic oxygen evolution reaction, *Appl. Surf. Sci.*, 2025, **692**, 162718.
24 J. Yuan, *et al.*, Paired array electrocatalyst coupling NiFe-MOF and NiFe-LDH for boosting oxygen evolution reaction, *J. Alloys Compd.*, 2024, **1005**, 176136.
25 G. Y. Abo El-Reesh, *et al.*, Novel synthesis of Ni/Fe layered double hydroxides using urea and glycerol and their enhanced adsorption behavior for Cr(VI) removal, *Sci. Rep.*, 2020, **10**(1), 587.
26 Y. Li, *et al.*, Morphology Evolution of NiFe Layered Double-Hydroxide Nanoflower Clusters from Nanosheets: Controllable Structure–Performance Relation for Green Energy Storage, *Energy Technol.*, 2024, **12**(1), 2300749.
27 N. Mamdouh, *et al.*, Effect of ZIF-67-derived Co_3O_4 on the activity of CNTs/$NiCo_2O_4$ nanocomposite for methanol oxidation reaction, *Int. J. Hydrogen Energy*, 2024, **93**, 878–887.
28 S. Lowell, *et al.*, Adsorption Isotherms, in *Characterization of Porous Solids and Powders: Surface Area, Pore Size and Density*, ed. S. Lowell, et al., Springer, Netherlands, Dordrecht, 2004, pp. 11–14.
29 L.-M. Cao, *et al.*, Template-directed synthesis of sulphur doped NiCoFe layered double hydroxide porous nanosheets with enhanced electrocatalytic activity for the oxygen evolution reaction, *J. Mater. Chem. A*, 2018, **6**(7), 3224–3230.
30 S. Sundriyal, *et al.*, High-Performance Symmetrical Supercapacitor with a Combination of a ZIF-67/rGO Composite Electrode and a Redox Additive Electrolyte, *ACS Omega*, 2018, **3**(12), 17348–17358.
31 Z. Liu, *et al.*, Nanostructured Co_3O_4@NiFe-LDH heterojunction catalysts for improving oxygen evolution reaction in alkaline environment, *J. Alloys Compd.*, 2024, **983**, 173837.
32 Z. Zheng, *et al.*, Microcrystallization and lattice contraction of NiFe LDHs for enhancing water electrocatalytic oxidation, *Carbon Energy*, 2022, **4**(5), 901–913.
33 C. Yin, *et al.*, Regulating the electronic state of SnO_2@NiFe-LDH heterojunction: Activating lattice oxygen for efficient oxygen evolution reaction, *Fuel*, 2024, **370**, 131762.
34 W. Li, *et al.*, Monodisperse SnO_2/Co_3O_4 nanocubes synthesized via phase separation and their advantages in electrochemical Li-ion storage, *Ionics*, 2020, **26**(12), 6125–6132.
35 S. Wang, *et al.*, Electrochemical impedance spectroscopy, *Nat. Rev. Methods Primers*, 2021, **1**(1), 41.
36 A. J. Bard, L. R. Faulkner, and H. S. White, *Electrochemical Methods: Fundamentals and Applications*, John Wiley & Sons, 2022.